Journal of Nanobiotechnology

RESEARCH

Open Access

β-Cyclodextrin-optimized supramolecular nanovesicles enhance the droplet/foliage interface interactions and inhibition of succinate dehydrogenase (SDH) for efficient treatment of fungal diseases

Deng-Xuan Guo[1†], Li Song[1†], Jing-Han Yang[1], Xin-Yu He[1], Pan Liu[1] and Pei-Yi Wang[1*]

Abstract

Background Plant fungal diseases present a major challenge to global agricultural production. Despite extensive efforts to develop fungicides, particularly succinate dehydrogenase inhibitors (SDHIs), their effectiveness is often limited by poor retention of fungicide droplets on hydrophobic leaves. The off-target losses and unintended release cause fungal resistance and severe environmental pollution.

Results To update the structure of existing SDHIs and synchronously realize the efficient utilization, we have employed a sophisticated supramolecular strategy to optimize a structurally novel SDH inhibitor (AoH25), creating an innovative supramolecular SDH fungicide (AoH25@*β*-CD), driven by the host-guest recognition principle between AoH25 and *β*-cyclodextrin (*β*-CD). Intriguingly, AoH25@*β*-CD self-assembles into biocompatible supramolecular nanovesicles, which reinforce the droplet/foliage (liquid-solid) interface interaction and the effective wetting and retention on leaf surfaces, setting the foundation for enhancing fungicide utilization. Mechanistic studies revealed that AoH25@*β*-CD exhibited significantly higher inhibition of SDH (IC_{50} = 1.56 μM) compared to fluopyram (IC_{50} = 244.41 μM) and AoH25 alone (IC_{50} = 2.29 μM). Additionally, AoH25@*β*-CD increased the permeability of cell membranes in *Botryosphaeria dothidea*, facilitating better penetration of active ingredients into pathogenic cells. Further experimental outcomes confirmed that AoH25@*β*-CD was 88.5% effective against kiwifruit soft rot at a low-dose of 100 μg mL^{-1}, outperforming commercial fungicides such as fluopyram (52.4%) and azoxystrobin (65.4%). Moreover, AoH25@*β*-CD showed broad-spectrum bioactivity against oilseed rape sclerotinia, achieving an efficacy of 87.2%, outstripping those of fluopyram (48.7%) and azoxystrobin (76.7%).

†Deng-Xuan Guo and Li Song contributed equally to this work.

*Correspondence:
Pei-Yi Wang
pywang@gzu.edu.cn; pywang888@126.com

Full list of author information is available at the end of the article

Conclusion This innovative approach addresses key challenges related to fungicide deposition and resistance, improving the bioavailability of agricultural chemicals. The findings highlight AoH25@β-CD as a novel supramolecular SDH inhibitor, demonstrating its potential as an efficient and sustainable solution for plant disease management.

Keywords Supramolecular SDH inhibitors, Foliar deposition, Antifungal, Improved utilization

Graphical Abstract

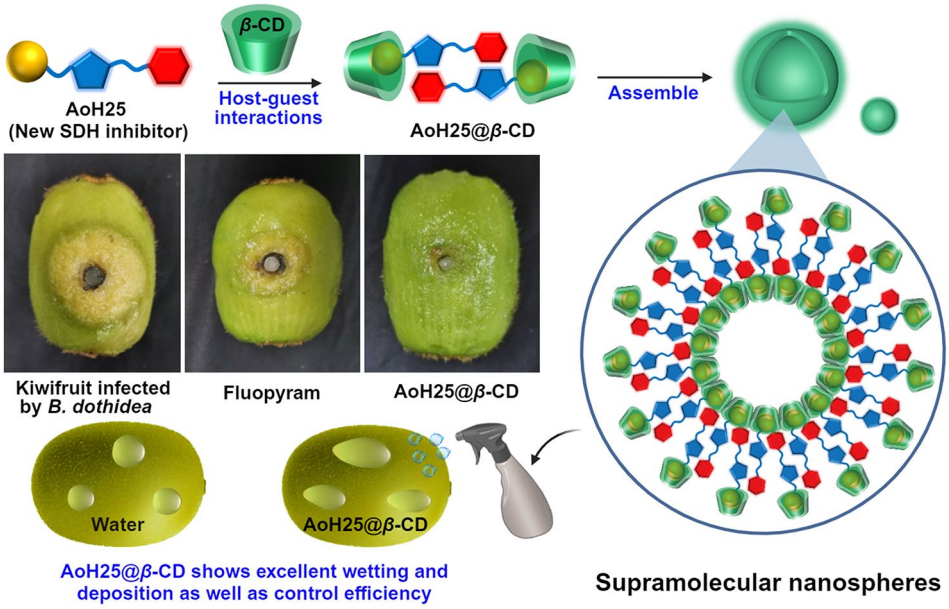

Introduction

Plant diseases caused by various pathogenic fungi pose a significant threat to global food security, leading to an annual crop loss of approximately 20% and further intensifying the food crisis in many countries and regions [1–4]. Fungicides are a powerful weapon in modern agriculture for combating plant diseases [5, 6]. Among the various fungicides in existence, succinate dehydrogenase inhibitors (SDHIs), including fluopyram, carboxin, penthiopyrad, fluxapyroxad, flubeneteram and so on, have garnered significant attention and wide application [7]. These fungicides target and inhibit succinate dehydrogenase (SDH) of pathogenic fungi, which is an essential enzyme in the tricarboxylic acid (TCA) cycle and mitochondrial electron transfer. Through this privileged mechanism, fungal energy production and respiration are severely disrupted, thereby effectively impairing fungal survival, proliferation, and infection [8, 9]. Currently, SDHIs are a crucial strategic resource in plant disease management [10]. However, the hydrophobic nature of plant surfaces poses a significant challenge to the effective utilization of traditional SDH fungicides. Upon contact with the leaf surface during spraying, fungicide droplets often exhibit undesirable behaviors such as bouncing, splashing and rolling, which result in low foliar retention, high off-target movement, and inefficient utilization [11]. Consequently, this inefficiency necessitates higher dosages and more frequent applications to achieve effective disease control. However, these practices not only escalate costs and environmental impact, but also accelerate the development of resistance in these fungi, undermining long-term disease management strategies [12]. In point of fact, many species of fungal strains, exemplified by *Botrytis cinerea*, *Corynespora cassiicola*, *Alternaria alternata*, and *Aspergillus oryzae*, have been reported to confer resistance to traditional SDHIs [13–16]. Therefore, it is indispensable to update the chemical structure of existing SDHIs and synchronously realize the efficient foliar retention and agrochemical utilization.

Promisingly, supramolecular self-assembly (SSA) systems demonstrate significant potential in addressing the above-mentioned challenges [17–19]. By utilizing various non-covalent interactions—such as electrostatic forces, hydrogen bonds, hydrophobic effects, van der Waals forces, and host-guest recognition—SSA systems organize active small/macrocyclic molecules into stable and ordered assemblies [20]. Through this manipulation, the achieved supramolecular assembly often has optimal physicochemical and biocompatible properties, thus providing an opportunity to improve the liquid-solid (droplet-foliage) interface interaction [21, 22]. Supramolecular assemblies in solution can reduce surface

tension, optimize contact angles and improve viscoelasticity, ensuring fungicide droplets to spread and deposit uniformly across hydrophobic leaf surfaces [23, 24]. This advisable strategy not only enhances the agrochemical utilization rate, but also relieves environmental impact to non-target organisms and fragile ecosystems.

Among the existing supramolecular strategies, host-guest recognition principle offers unique advantages in constructing assemblies that extend beyond the general properties of supramolecules [25]. The precise and selective interactions between host molecules and their guests enables a sophisticated control over the assembly process. Such characteristics have led to extensive applications in material science, biomedicine, and environmental science [26–28]. In host-guest chemistry, carbohydrate-based macrocycles—cyclodextrins (CDs), owning hydrophilic polyhydroxy surfaces and relatively hydrophobic cavities, are particularly well-suited for forming host-guest combinations with hydrophobic guest molecules [29–31]. These distinctive features make CDs an ideal choice for creating stable and biocompatible supramolecular assemblies. Of the three commonly used CDs—α-CD, β-CD and γ-CD, seven-membered β-CD is particularly noteworthy [32]. Not only is it the most cost-effective to produce, but its moderate cavity size is perfectly suited for accommodating a wide range of guest molecules, thereby facilitating the formation of stable and effective supramolecular assemblies [33]. A particularly fascinating application of β-CD is its combination with adamantane [34]. The resulting β-CD/adamantane complexes usually showcases a remarkable synergy in enhancing the water-solubility, stability, biocompatibility and biological functions, synchronously assembling into multifunctional assemblies with different morphologies [35]. Furthermore, adamantane derivatives have been extensively explored as potential therapeutic agents, demonstrating practical efficacy in treating viral infections, bacterial diseases, and cancer cell proliferation [36–38]. Inspired by those in-depth surveys, developing novel antifungal agents based on adamantane skeleton modification is feasible to update the chemical structure of existing SDHIs. However, their hydrophobic nature limits their solubility and bioavailability, posing challenges for their effective use in biological systems. Encouragingly, we will employ the intelligent β-CD-involved host-guest manipulation to optimize the physicochemical and biological properties of active adamantane-based compounds, thereby creating biocompatible multifunctional supramolecular assemblies for fungal diseases management.

Building on the above-mentioned design philosophy, a series of novel adamantane derivatives were synthesized and biologically evaluated. Whereafter, a highly bioactive adamantane-functionalized 1,3,4-oxadiazole hydrazide (AoH25) was screened out as the optimal antifungal agent targeting SDH. Then, through the host-guest recognition principle, AoH25 was optimized by the macrocyclic oligosaccharide—β-CD, producing an innovative supramolecular SDH inhibitor (AoH25@β-CD), which spontaneously assembled into supramolecular nanovesicles. These nanoscale assemblies inherit principal advantages of both AoH25 and β-CD, thus reinforcing the droplet/foliage interface interaction and the effective wetting and retention on leaf surfaces, setting the foundation for enhancing fungicide utilization (Scheme 1). Additionally, the self-assembled AoH25@β-CD enhances the SDH inhibitory activity, contributing to its overall antifungal efficacy. In brief, this supramolecular optimization approach holds promise for constructing multipurpose fungicides in controlling fungal infections and simultaneously paves the way for more effective and sustainable agricultural practices.

Methods

In vitro antifungal evaluation

The antifungal activities of target compounds were assessed against six plant pathogenic fungi using the mycelial growth inhibition method [39]. Fluopyram (FP) and azoxystrobin (AZX) served as positive control agents, which were purchased from Energy-Chemical of Saen-Chemical-Technology (Shanghai) Co., Ltd., with a high purity (≥98%, HPLC). The wild-type fungal strains, including *Botryosphaeria dothidea* (*B. dothidea*), *Sclerotinia sclerotiorum* (*S. sclerotiorum*), *Fusarium oxysporum* (*F. oxysporum*), *Gibberella zeae* (*G. zeae*), *Magnaporthe grisea* (*M. grisea*) and *Rhizoctonia solani* (*R. solani*), were provided and isolated by Prof. Wenneng Wu from Food and Pharmaceutical Engineering Institute, Guiyang University [40–42]. Generally, 0.1 mL stock solutions (50 mg mL^{-1}) of target compounds in DMSO with 0.9 mL DMSO was added into 9 mL 0.1% tween-20 aqueous solution. Then, this mixture was added into 90 mL potato dextrose agar (formula: 400 g potato soup, 40 g glucose, 40 g agar powder in 2.0 L distilled water, sterilized with high temperature) to create 50 μg mL^{-1} solid test mediums (containing 1% DMSO). After that, 0.5 cm agar disk containing the fungal strain was placed on the 10 mL of the above solid test medium containing target compounds and positive controls (the dose was 50 μg mL^{-1}), each group was set to repeat three times. Subsequently, all groups were cultured in a climate chamber at 25–28 °C until the average colony diameter of the 1% DMSO control group reached 6.0–6.5 cm. Inhibition percentages were calculated using the formula: inhibition (%) = [(CK - C_1) / (CK −0.5)] × 100, where C_1 represents the average colony diameter for the treatment group, and CK is the average colony diameter of an equal volume of aqueous solution containing 1% DMSO. For compounds demonstrating significant initial inhibition, EC_{50} values

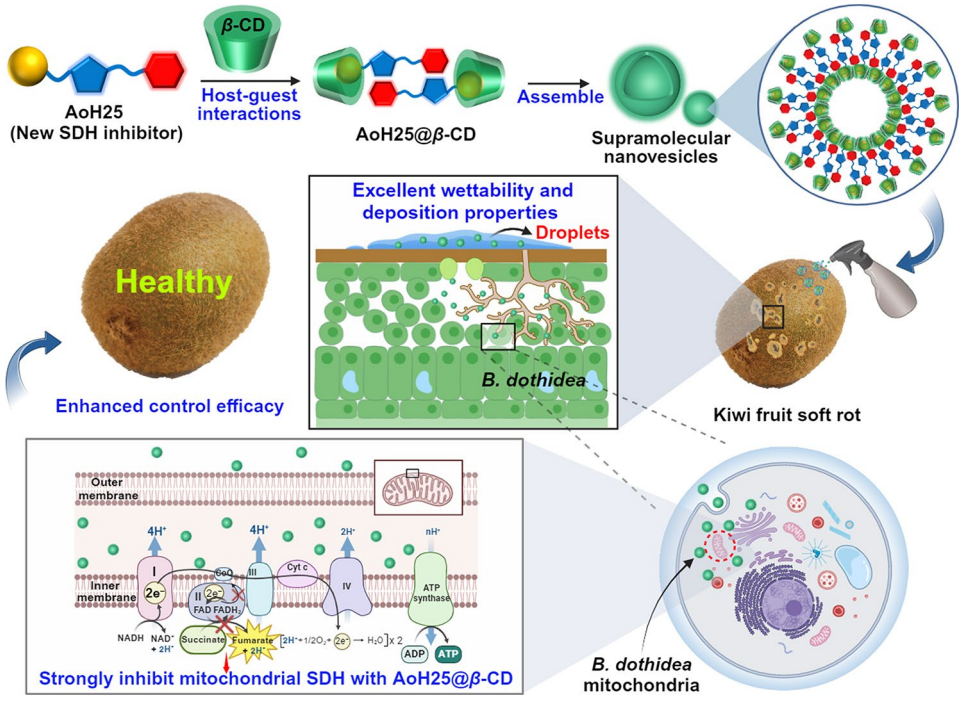

Scheme 1 Schematic depiction of constructing fungicidal supramolecular nanovesicles (AoH25@*β*-CD) to improve droplet wetting and deposition as well as efficiently inhibit fungal mitochondrial SDH

were determined. Stock solutions (50 mg mL^{-1}) of target compounds were diluted to a series of concentrations of 25, 12.5, 6.25, 3.125, and 1.5625 μg mL^{-1} in 10 mL solid nutrient broth medium using the method mentioned above. The corresponding EC_{50} values were calculated using Excel 2016.

Investigation of the antifungal mechanism

Molecular docking experiment [43]. Compound AoH25 and the commercial fungicide fluopyram were structurally drawn using ChemDraw 3D Pro. The "Calculations" option was selected with "MM2" to minimize energy, and the structures were saved in mol2 format. The SDH crystal structure (PDB code: 2FBW) was sourced from the RCSB Protein Data Bank (http://www.rcsb.org). Following the SYBYL-X 2.1.1 software docking protocol, the SDH protein was prepped by extracting ligands, removing water molecules, and adding hydrogen atoms. Molecular docking of the small molecules with the protein was executed. The results were visualized and analyzed using PyMOL software.

SEM morphology of *B. dothidea* [44]. The fungal strain *B. dothidea* was cultivated in a potato dextrose broth (PDB) medium containing AoH25@*β*-CD and AoH25 with an effective concentration of 50 μg mL^{-1} for 48 h at 28 °C in a shaker. Meanwhile, 1% DMSO (the solvent control) was set as the control group. After incubation, the *B. dothidea* cells were rinsed three times with PBS (pH 7.2). The cells were then fixed overnight at 4 °C using 2.5% glutaraldehyde and dehydrated through a graded ethanol series and pure tert-butanol. Following dehydration and drying, the mycelia were gold-coated for imaging.

The target compound AoH25, which has significant activity against *B. dothidea*, was tested for SDH inhibitory activity [45]. The commercial fungicide FP serves as a positive control. The SDH enzyme was extracted and its activity was determined according to the instructions of the SDH activity assay kit (BC0955, Solarbio, Beijing, China). Dichlorophenol indole phenol (DCPIP) was used as the substrate, and the reduction product, DCPIPH2, was formed during the process. In the PDB medium containing different concentrations of AoH25 and FP, fungal discs of *B. dothidea* were added and incubated at 28 °C with shaking at 180 rpm for 48 h. After incubation, the mycelium was centrifuged at 8500 rpm for 10 min to remove the supernatant, and the remaining mycelium was collected. The mycelium was washed several times with PBS, then ground thoroughly using a mortar and pestle on ice. This was followed by centrifugation at 11,000 rpm at 4 °C for 10 min. The supernatant was collected and kept on ice for subsequent SDH activity determination according to the kit instructions.

The impact of the compounds on the membrane permeability of *B. dothidea* mycelial cells was assessed via the conductivity method [46]. The fungus was cultured in PDB medium and incubated at 28 °C with shaking at 180 rpm for 4 days. After incubation, the mycelium was filtered, washed with sterile water, and filtered

again. Subsequently, 1.0 g of mycelium was placed into a 50 mL centrifuge tube, and 20 mL of compounds (25 μg mL^{-1} and 50 μg mL^{-1} solutions) were added. Sterile water served as the control. Each treatment was repeated three times. The initial conductivity (J_0) was measured using a conductivity meter. Conductivity values (J_1) were recorded at 1-hour intervals for up to 7 h at room temperature. After boiling and cooling the samples, the final conductivity (J_2) was determined. The relative conductivity was calculated as follows:

$$\text{Relative Conductivity (\%)} = \frac{J_1 - J_0}{J_2 - J_0} \times 100$$

Investigation of droplet behavior of supramolecular inclusion on plant surfaces

Contact angle assay [47]. The contact angle measuring instrument was used to measure the contact angle of all the samples droplets (water, *β*-CD, AoH25 and AoH25@*β*-CD). During the test, 10 μL droplets were added vertically to the surface of oilseed rape leaves and kiwi fruit peel using a microinjector. Next, the image of the droplet is captured using JC 2000D1 contact angle instrument.

Liquid holding capacities (LHC) assay [48]. The related leaves or fruit peels with 1.0 cm in diameter, were cut from oilseed rape leaves or kiwi fruits, respectively. Then, these samples were immersed in solutions of water, *β*-CD, AoH25 and AoH25@*β*-CD at a concentration of 200 μg mL^{-1}. After 20 s, the corresponding leaves or fruit peels were lifted vertically with tweezers until no droplets dropped, and their mass was measured using an analytical balance. The LHC was calculated using the following equation after performing all tests three times:

$$\text{LHC} = (M_1 - M_0)/S$$

The weight of the leaves or fruit peels before and after soaking are represented by M_0 and M_1, respectively, and S is the surface area of the leaves or fruit peels.

Droplet impact experiment [49]. The dynamic sliding and bounding experiments of droplets containing water, *β*-CD, AoH25, and AoH25@*β*-CD on oilseed rape leaves and kiwi fruit peel from a height of 15 cm was recorded using a Nikon Cyclona-2-2000-C high-speed camera at 2000 fps. Each sample had a concentration of 200 μg mL^{-1}. Parameters were obtained by analyzing the video footage with the i-SPEED suite software.

Dispersion and deposition on the leaves or fruit peels. The surface morphology of oilseed rape leaves and kiwi fruit peel was observed using SEM. First, 20 μL of 200 μg mL^{-1} AoH25 and AoH25@*β*-CD droplets were sprayed onto oilseed rape leaves and kiwi fruit peel supported on a carrier stage. After drying at room temperature, the dispersion state was observed using SEM.

The bioactivity assessment of AoH25@*β*-CD against Kiwi fruits soft rot

The bioactivity of tested agents against *B. dothidea* was performed on kiwi fruit [50]. For the protective activity assay, healthy kiwi fruits were sprayed with compound AoH25 and complex AoH25@*β*-CD (100 μg mL^{-1}). Then, all samples were cultivated for 24 h at 25 °C. Later, a 5 mm wound was made on the equatorial position of kiwifruit with a sterile needle, and the *B. dothidea* strain (0.5 cm agar disk) was inoculated on the wound surface. Regarding the curative trials, kiwi fruits were first inoculated with *B. dothidea* using the same method mentioned above. After incubating at 25 °C for 24 h, all the samples were sprayed with compound AoH25 and complex AoH25@*β*-CD (100 μg mL^{-1}), respectively. The outcomes were measured as diameters of lesions after incubation for 4 days. FP and AZX with a dose of 100 μg mL^{-1} were used as positive controls. In addition, 0.1% tween-20 was used to improve the water-solubility of compounds AoH25, FP, and AZX. The disease control efficacy (%) was determined using the formula $(c–d)/(c–0.5)\times100$, where "c" represents the diameter (cm) of the control group (0.4% DMSO aqueous solution), and "d" indicates the diameter (cm) of the treatment group. Each experiment was conducted in triplicate.

In vivo trials against rape sclerotinia rot

The fungicidal activity of various agents against *S. sclerotiorum* was evaluated on rape leaves through in vivo trials [51]. For the protective activity assay, healthy rape leaves were treated with AoH25 and AoH25@*β*-CD (100 μg mL^{-1}), followed by incubation at 25 °C for 24 h. Then, 0.5 cm agar disk containing the fungal strain *S. sclerotiorum* was placed near the center of the leaves. For the curative activity assay, healthy rape leaves were first inoculated with 0.5 cm agar disk containing *S. sclerotiorum*. After incubating at 25 °C for 24 h, all the samples were sprayed with AoH25 and AoH25@*β*-CD (100 μg mL^{-1}). Lesion diameters were measured after 4 days of incubation at 25 °C. Fluopyram (100 μg mL^{-1}) and azoxystrobin (100 μg mL^{-1}) in 0.1% tween-20 solutions served as positive controls. The disease control efficacy (%) was calculated using the formula $(c-d)/(c-0.5)\times100$, where "c" is the lesion diameter (cm) in the control group (0.4% DMSO aqueous solution), and "d" is the lesion diameter (cm) in the treatment group. Each treatment was performed in triplicate.

Statistical analysis

The used analytical tool was SPSS Statistics 27. Error bars indicate the means ± SD. One-way analysis of variance (ANOVA) was used to analyze the differences between the different components, and a different letter was

considered significant ($p<0.05$). The related statement was supplemented in the revised manuscript.

Results and discussion

Molecular design and in vitro antifungal assays of novel small molecules AoH1-AoH26

The design of promising antifungal molecules requires synthetic simplicity and potent bioactivity towards the specific target. Our previous works have found 1,3,4-oxadiazole-2-carbohydrazide derivatives are potential SDHIs and exhibit good antifungal efficacy towards plant pathogenic fungi [52]. In this study, the versatile adamantane scaffold was incorporated into the 1,3,4-oxadiazole-2-carbohydrazide to efficiently acquire novel antifungal compounds as potential SDHIs. Given that, we synthesized a series of new adamantane derivatives (AoH1-AoH26) containing a 1,3,4-oxadiazole-2-carbohydrazide fragment using a two-step method (Scheme 2). The first step involved the cyclization of adamantane-1-carbohydrazide or 2-(adamantyl)-acethydrazide with diethyl oxalate in the presence of phosphorus oxychloride ($POCl_3$) at 85 °C, forming a key 1,3,4-oxadiazole ring. Next, this intermediate was reacted with various phenylhydrazines in dimethylformamide (DMF) at 100 °C to afford target compounds (AoH1-AoH26). Finally, their molecular structures were rigorously characterized and confirmed using nuclear magnetic resonance (NMR) and high-resolution mass spectrometry (HRMS) (Fig. S3-S92).

To gain an insight into the in vitro bioactivity of achieved compounds, AoH1-AoH26 were evaluated against six pathogenic fungi, including *B. dothidea*, *S. sclerotiorum*, *F. oxysporum*, *G. zeae*, *M. grisea* and *R. solani* by mycelium growth rate method [53]. Based on the preliminary screening results, the inhibitory rate of most synthesized compounds against *B. dothidea* and *S. sclerotiorum* exceeded 70% at a concentration of 50 μg mL^{-1} (Table 1 and Table S1). Further bioassay results demonstrated that these bioactive compounds (except AoH2-AoH8 and AoH16-AoH21) exhibited superior antifungal activities against *B. dothidea*, with EC_{50} values ranging from 0.14 to 6.60 μg mL^{-1}. In particular, compounds AoH10, AoH23, and AoH25 afforded the optimal EC_{50} values of 0.14 ~ 0.15 μg mL^{-1}, which were quite better than those of fluopyram (FP, 16.3 μg mL^{-1}) and azoxystrobin (AZX, 11.8 μg mL^{-1}). For the anti-*S. sclerotiorum* activity, compounds AoH10, AoH12-AoH13, and AoH22-AoH26 provided a EC_{50} value range of 1.43 ~ 7.90 μg mL^{-1}. Among them, AoH25 gave the minimum EC_{50} value of 1.43 μg mL^{-1}, obviously surpassing the commercial fungicides FP (>50 μg mL^{-1}) and AZX (18.6 μg mL^{-1}). Moreover, compound AoH25 exhibited broad-spectrum bioactivity against *F. oxysporum*, *G. zeae*, and *M. grisea* with EC_{50} values of 3.40, 0.77, and 5.05 μg mL^{-1}, respectively (Tables S2-S3). The preliminary structure-activity relationship was summarized as follows. (1) Introducing a methylene bridge between adamantane and 1,3,4-oxadiazole often enhances the antifungal activity. (2) The position of the halogen on the benzene ring significantly affects the biological activity, such as the anti-*B. dothidea* activity of AoH25 (4-Cl, 0.14 μg mL^{-1}) and AoH24 (3-Cl, 3.99 μg mL^{-1}). (3) A strong electron-donating group obviously reduces the anti-*B. dothidea* activity, such as AoH17 (4-OCH_3, > 25 μg mL^{-1}) and

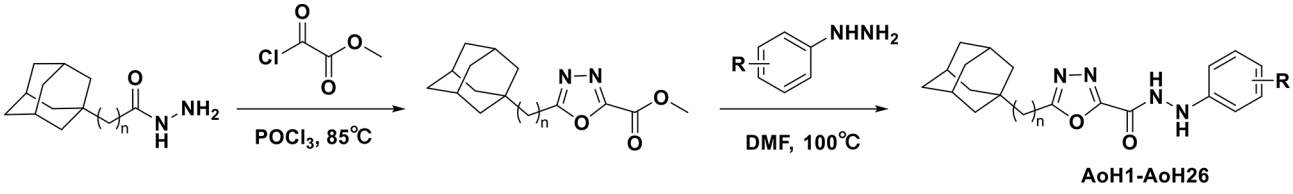

Compounds	n	R	Compounds	n	R
AoH1	0	H	AoH14	1	H
AoH2	0	4-CH_3	AoH15	1	4-CH_3
AoH3	0	4-$C(CH_3)_3$	AoH16	1	4-$C(CH_3)_3$
AoH4	0	4-OCH_3	AoH17	1	4-OCH_3
AoH5	0	2-F	AoH18	1	2-F
AoH6	0	3-F	AoH19	1	3-F
AoH7	0	4-F	AoH20	1	4-F
AoH8	0	2,4-2F	AoH21	1	2,4-2F
AoH9	0	2,5-2F	AoH22	1	2,5-2F
AoH10	0	3,4-2F	AoH23	1	3,4-2F
AoH11	0	3-Cl	AoH24	1	3-Cl
AoH12	0	4-Cl	AoH25	1	4-Cl
AoH13	0	3,4-2Cl	AoH26	1	3,4-2Cl

Scheme 2 Synthesis of target compounds AoH1-AoH26

Table 1 Preliminary inhibition rate and EC_{50} values of some title compounds against *B. dothidea* and *S. sclerotiorum*

Compds	*B. dothidea*			*S. sclerotiorum*		
	Inhibition ratio (%) (50 μg mL^{-1})	Regression equation	EC_{50} (μg mL^{-1})	Inhibition ratio (%) (50 μg mL^{-1})	Regression equation	EC_{50} (μg mL^{-1})
AoH1	100	y = 1.462x + 4.132	3.92 ± 0.11	76.3 ± 1.1	—	>25
AoH9	100	y = 0.491x + 4.982	1.10 ± 0.21	76.5 ± 1.2	—	>25
AoH10	100	y = 1.288x + 6.048	0.15 ± 0.01	100	y = 1.107x + 4.006	7.90 ± 0.37
AoH11	100	y = 1.044x + 4.614	2.34 ± 0.04	46.8 ± 2.4	—	>50
AoH12	100	y = 1.112x + 5.721	0.22 ± 0.12	100	y = 1.954x + 4.431	1.95 ± 0.11
AoH13	100	y = 1.532x + 4.620	1.77 ± 0.23	100	y = 1.811x + 3.915	3.97 ± 0.22
AoH14	100	y = 1.226x + 4.374	3.24 ± 0.37	72.4 ± 3.2	—	>25
AoH15	100	y = 1.203x + 4.014	6.60 ± 1.04	73.0 ± 2.1	—	>25
AoH22	100	y = 1.413x + 5.052	0.92 ± 0.04	100	y = 1.782x + 3.862	4.35 ± 0.57
AoH23	100	y = 1.211x + 6.009	0.15 ± 0.01	100	y = 1.331x + 4.363	3.01 ± 0.38
AoH24	100	y = 1.352x + 4.188	3.99 ± 0.28	100	y = 1.582x + 4.022	4.15 ± 0.25
AoH25	100	y = 0.743x + 5.643	0.14 ± 0.06	100	y = 1.350x + 4.791	1.43 ± 0.18
AoH26	100	y = 1.183x + 4.712	1.75 ± 0.07	100	y = 2.063x + 4.168	2.53 ± 0.17
FP	64.0 ± 1.3	y = 0.719x + 4.128	16.3 ± 0.9	46.5 ± 0.3	—	>50
AZX	70.7 ± 0.9	y = 0.451x + 4.516	11.8 ± 0.8	74.2 ± 0.1	y = 0.652x + 4.172	18.6 ± 0.7

Note FP (commercial fluopyram); AZX (commercial azoxystrobin), the EC_{50} value of antifungal activity is indicated as means ± SD (standard deviation)

AoH14 (-H, 3.24 μg mL^{-1}). (4) Multiple substituents on the benzene ring decreases the antifungal effect against *B. dothidea*, exemplified by AoH26 (3,4-diCl, 1.75 μg mL^{-1}) and AoH25 (4-Cl, 0.14 μg mL^{-1}).

Among all tested compounds, AoH25, featuring a cheap 4-chlorophenyl substituent, demonstrated the most substantial inhibitory effects against tested pathogenic fungi, which was selected as a promising candidate for the following treatment of fungal diseases. However, compound AoH25, as a representative, shows weak water-solubility and biocompatibility, significantly limiting its bioavailability in practical applications. Therefore, we employ a β-CD-involved host-guest recognition supramolecular strategy to optimize the physicochemical and biological properties of AoH25 and eventually create biocompatible supramolecular assemblies for efficient foliar deposition and fungicide utilization (Scheme 1).

Characterization, driving forces, and self-assembling process for β-CD-optimized supramolecular nanovesicles (AoH25@β-CD)

The biocompatible macrocyclic oligosaccharide—β-CD was utilized to optimize the small molecule AoH25 through the specific host-guest envelopment. Briefly, the guest molecule AoH25 (20.0 μL, 0.13 M) in tetrahydrofuran (THF) solvent was added dropwise to 5.0 mL of deionized water containing the macrocyclic host β-CD (0.52 mmol). The final effective concentration is 200 μg mL^{-1} (0.52 mmol) with a molar ratio of AoH25 : β-CD = 1:1. After natural evaporation of THF, the self-assembled supramolecular complexes (AoH25@β-CD) formed. In this process, the self-assembly behavior of AoH25 with β-CD, including driving forces, packaging location, stoichiometric ratio and micro-morphology change, was probed by ^{1}H NMR titration, UV-vis titration, HRMS, dynamic light scattering (DLS), scanning electron microscope (SEM) and molecular dynamics (MD) simulation.

The ^{1}H NMR titration spectra revealed that the proton signals of H_a-H_i (adamantyl) experienced a significant downfield shift ($\Delta\delta$ = 0.11 ~ 0.21 ppm) after the introduction of 1.0 equiv. β-CD, indicating the inclusion of adamantane moiety of AoH25 into the β-CD cavity (Fig. 1a). Specifically, the proton signals of H_j (-CH_2-) adjacent to the adamantane moiety showed an apparent upfield shift ($\Delta\delta$ = -0.05 ppm), indicating this methylene fragment was located outside the cavity of β-CD, thus causing the deshielding effect. When the amount of β-CD was increased from 0.5 to 1.5 equiv., the chemical shifts provided a slight chemical shift, suggesting that β-CD successfully encapsulates the adamantane part of AoH25, consistent with literature reports [54, 55].

To gain further insights into the host-guest driving force, we performed the UV/vis titration spectra of AoH25 with β-CD (Fig. 1b). As β-CD was gradually added, the UV absorption at 255 ~ 360 nm diminished. This reduction is attributed to the successful encapsulation of adamantane moiety within the β-CD cavity, resulting in increased solubility and dispersion of the guest molecules (AoH25). Moreover, as the molar ratio reached 1:1, the UV change basically reached equilibrium, indicating a 1:1 binding ratio. The titration experiment also produced an Eq. $1/\Delta A = 0.0001184/[\beta\text{-CD}] + 2.0559$, which yielded a binding constant (Ka) of 1.7369×10^4 (Fig. 1c), underscoring the strong affinity between AoH25 and β-CD. Next, the molecular weight of the assembled product AoH25@β-CD was determined using HRMS. The spectrum showed two prominent

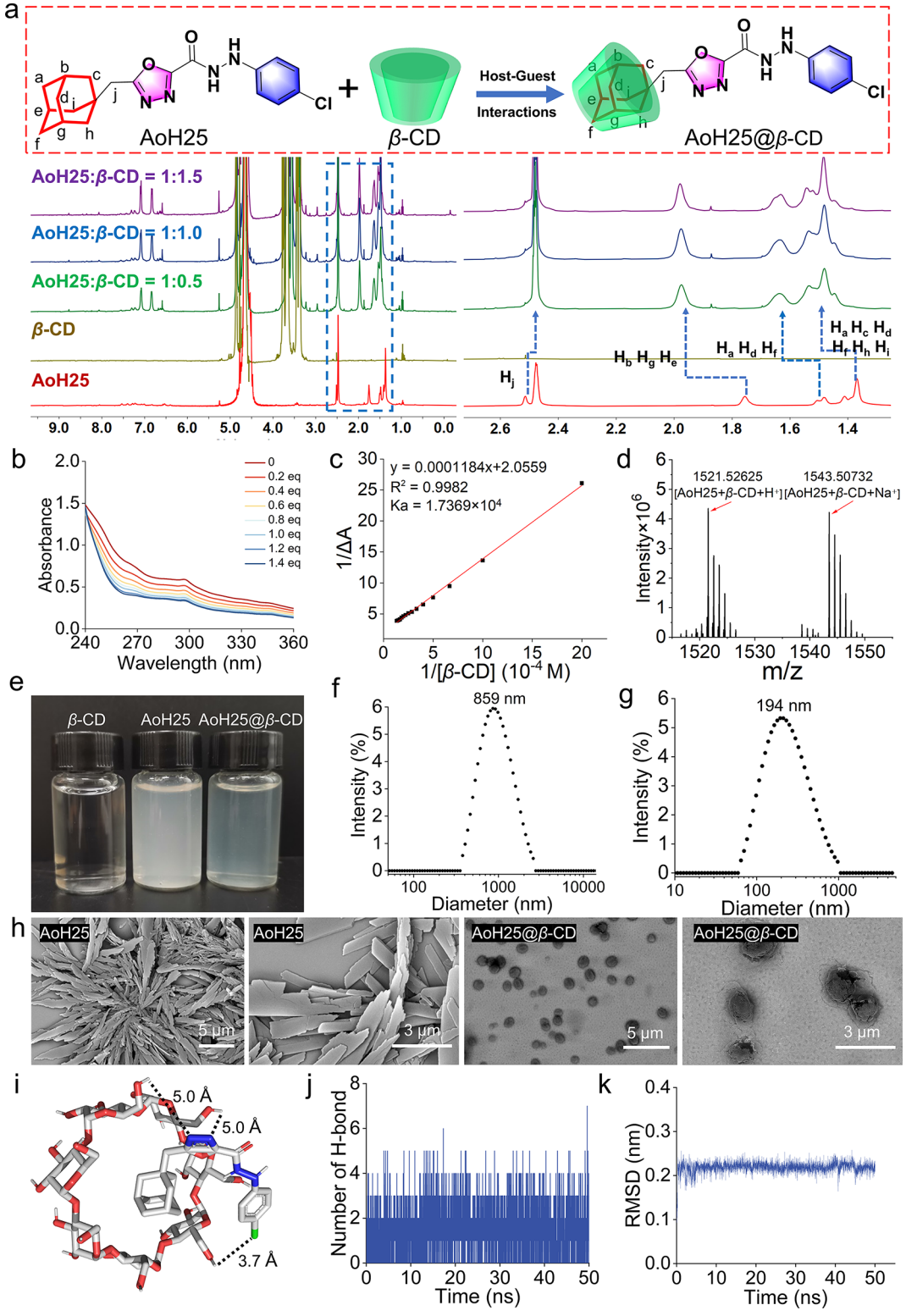

Fig. 1 The correlative characterization of AoH25@β-CD. (**a**) ^{1}H NMR titration spectra of AoH25 by β-CD with different molar ratios (1:0.5, 1:1, 1:1.5) in D_2O. (**b**) UV-vis absorption spectra of AoH25 (0.14 mM) with increasing the doses of β-CD (0 ~ 1.4 equiv.) in aqueous solution. (**c**) Benesi-Hildebrand plots of colorimetric $[\Delta A]^{-1}$. (**d**) HRMS of AoH25@β-CD. (**e**) Photographs of β-CD, AoH25, and AoH25@β-CD in aqueous solution at 200 μg mL^{-1}. (**f**, **g**) DLS profiles of AoH25 and AoH25@β-CD at 200 μg mL^{-1}. (**h**) SEM images of AoH25 and AoH25@β-CD at 200 μg/mL. (**i**) Molecular docking and binding sites of AoH25 with β-CD. (j) Number of H-bond in AoH25@β-CD during 50 ns MD simulations. (k) RMSD plots of AoH25@β-CD during 50 ns MD simulations

peaks at m/z 1521.5263 and 1543.5073, corresponding to [AoH25+*β*-CD+H^+] and [AoH25+*β*-CD+Na^+], respectively (Fig. 1d). Subsequently, the photographs of *β*-CD, AoH25, AoH25@*β*-CD in aqueous solution at 200 μg mL^{-1} were provided (Fig. 1e). It was evident that the AoH25 solution appeared turbid white, whereas the AoH25@*β*-CD solution was relatively more transparent after introducing the biocompatible macrocycle *β*-CD. This improvement is attributed to the hydrophilic *β*-CD encapsulating the hydrophobic adamantane moiety of AoH25, agreeing with the above-observed UV/vis titration result. Additionally, DLS measurements provided the sizes of the two types of nanoparticles (Fig. 1f and g). The average diameter of AoH25@*β*-CD was 194 nm, significantly smaller than the 859 nm observed for AoH25 alone. This reduction in size holds great promise for agricultural applications, as smaller nanoparticles possess a larger specific surface area, facilitating more uniform and extensive coverage on the leaf surface, thereby potentially enhancing the fungicidal effect. Moreover, smaller particle size may also improve the penetration of the AoH25, thus enhancing the overall efficacy in practical applications.

The self-assembled microscopic structures from single AoH25 and the newly formed supramolecule AoH25@*β*-CD were observed separately using SEM (Fig. 1h). AoH25 appears as dense sheets, with most sheets oriented towards a central point. This morphology is attributed to the nonpolar nature of the adamantane structure, causing AoH25 to self-aggregate and tightly stack in aqueous solution due to strong hydrophobic interactions. In contrast, AoH25@*β*-CD exhibits relatively dispersed spherical particles. The introduction of *β*-CD encapsulates the hydrophobic adamantane moiety of AoH25, significantly altering its spatial arrangement (Scheme 1). By reducing hydrophobic interactions, *β*-CD disrupts the formation of dense sheets, allowing the molecules to form more stable spherical aggregates in aqueous environments. These spherical aggregates minimize the exposure of hydrophobic regions to the solvent, thus reducing unfavorable hydrophobic interactions. Moreover, the abundant hydroxyl groups and oxygen ethers on *β*-CD strengthen the hydrogen bond interaction during molecular arrangement, so the building block—AoH25@*β*-CD tends to assemble into supramolecular nanovesicles. The stability of this supramolecular system was assessed by HPLC measurements at different storage periods under different storage temperatures. As shown in Fig. S1, after seven days of storage at 15 °C, 25 °C, and 35 °C, the peak area of AoH25@*β*-CD almost did not change significantly, confirming the stability of the current supramolecular system.

Molecular docking and molecular dynamics simulations are commonly used to explore the driving forces and stability of supramolecular systems [56]. Based on the molecular docking model shown in Fig. 1i, it is observed that the cyclodextrin cage structure encloses the adamantane moiety of AoH25. Subsequently, molecular dynamics simulations were conducted to analyze the changes in hydrogen bonds over time. Throughout the 0 to 50 ns simulation, the number of hydrogen bonds predominantly ranged from 1 to 3, indicating the presence of relatively stable hydrogen bond interactions within the system (Fig. 1j). Further analysis was performed to determine the existence of other driving forces in AoH25@*β*-CD apart from hydrogen bonds. As seen in Table S4, the van der Waals energy is -133.192 kJ/mol, signifying its significant role in maintaining the stability of the supramolecular complex. Additionally, the RMSD value of AoH25@*β*-CD fluctuated around 0.2 nm throughout the 0 to 50 ns period (Fig. 1k), demonstrating the structural stability of the AoH25@*β*-CD simulation system without notable conformational changes. These findings collectively confirm the successful fabrication of a novel biocompatible supramolecular nanoscale material (AoH25@*β*-CD), laying a solid foundation for promoting the efficient wetting and deposition of fungicide droplets on hydrophobic foliar surfaces and the sustained bioavailability in controlling fungal diseases.

Enhanced wetting and retention properties of carbohydrate-based nanoscale assemblies (AoH25@*β*-CD) on kiwifruit surfaces

The pathogenic *B. dothidea* is a chief culprit that causes the kiwi fruit soft rot, seriously harming the kiwifruit industry [57]. Before doing the in vivo antifungal efficacy of supramolecular material AoH25@*β*-CD, we conducted a comprehensive evaluation of its deposition performance on the hydrophobic surface of kiwifruit. The key parameters include contact angle measurements, spray observation, liquid holding capacity (LHC), droplet sliding analysis, and topological morphology on kiwifruit surface. Firstly, the contact angle of AoH25@*β*-CD on the kiwifruit surface was 57.5° (Fig. 2a), significantly lower than that of water (83.8°), *β*-CD (81.3°), and AoH25 (73.5°), indicating the achieving superior wettability after optimizing AoH25 by the biocompatible macrocyclic oligosaccharide—*β*-CD. Furthermore, after spraying AoH25@*β*-CD, AoH25, or *β*-CD droplets onto the kiwifruit, we found that AoH25@*β*-CD exhibited the smallest droplet size and most uniform distribution on the kiwifruit surface, consistent with contact angle test results and the following LHC detection. As shown in Fig. 2b, the retention amount of AoH25@*β*-CD on the kiwifruit peel was 32.7 mg/cm^2, significantly higher than that of single AoH25 (20.9 mg/cm^2) and other control groups, confirming that AoH25@*β*-CD droplets tend to adhere to the kiwifruit surface.

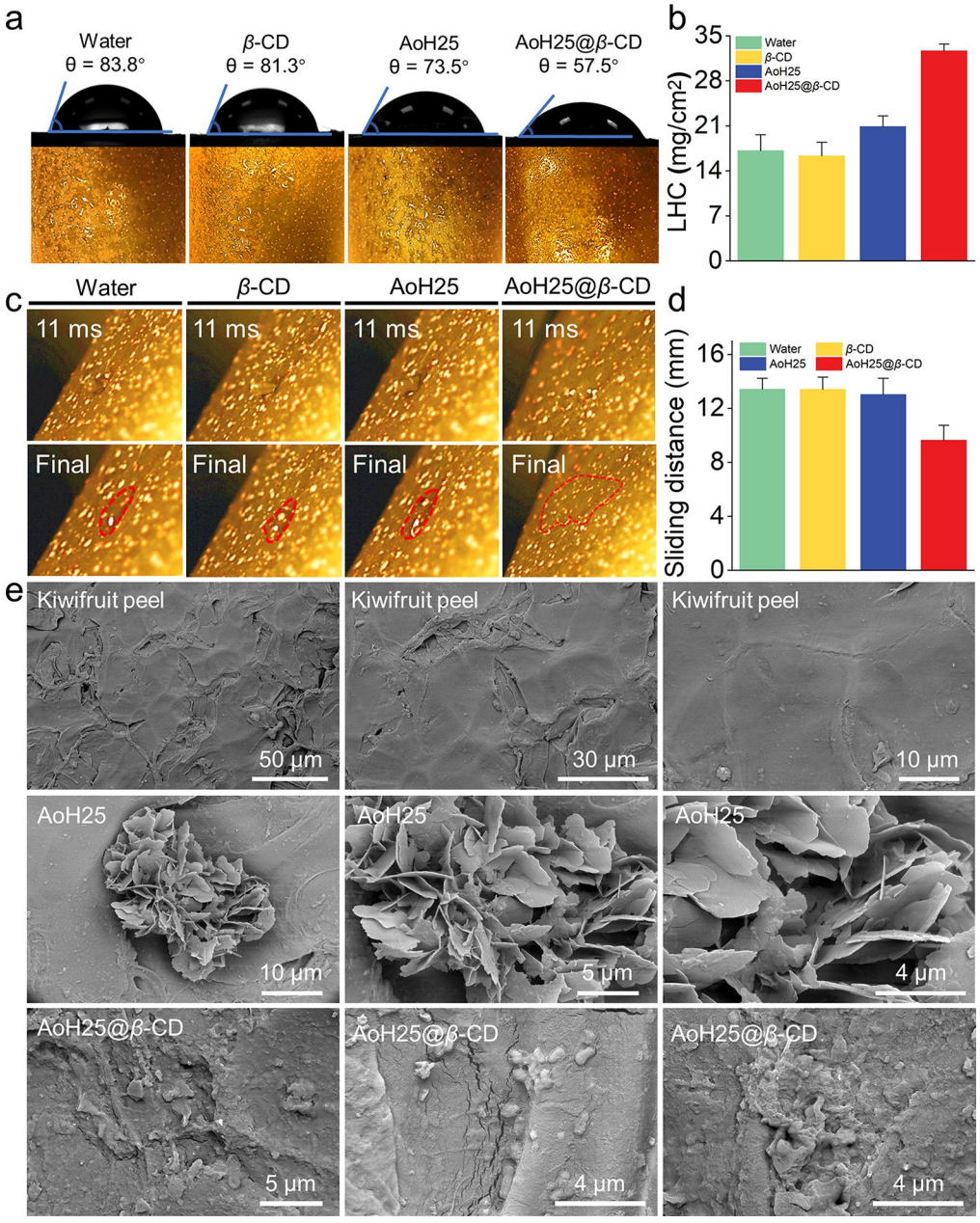

Fig. 2 (**a**) Contact angles of water, *β*-CD, AoH25, AoH25@*β*-CD droplets on kiwifruit peel at 200 *μ*g mL^{-1}. (**b**) Liquid holding capacity (LHC) of water, *β*-CD, AoH25, AoH25@*β*-CD after dipping in kiwifruit peel at 200 *μ*g mL^{-1}. (**c**) The kiwifruit peel is placed at 60°, the related droplets are released at a height of 15 cm and recorded by a high-speed camera, scale: 2 mm. (**d**) Sliding distance of water, *β*-CD, AoH25, AoH25@*β*-CD droplets on the kiwifruit peel. (**e**) SEM images of blank control, AoH25 and AoH25@*β*-CD deposited on kiwifruit peel at 200 *μ*g mL^{-1}

Considering that the low deposition efficiency of conventional pesticide droplets is mainly attributed to their rolling off the leaf surface, we inclined the kiwifruit at a 60° angle and released droplets of AoH25@*β*-CD and other treatment groups from a height of 15 cm to research their sliding behavior on the kiwifruit surface. This process was recorded with a high-speed camera and illustrated in Fig. 2c and Video S1. Upon the impact, all droplets rolled a certain distance before finally settling on the kiwifruit peel. Among them, the droplets of AoH25, water, and *β*-CD formed bulges, whereas AoH25@*β*-CD formed a thin and uniform water film on the kiwifruit surface. Figure 2d shows that the sliding distance of AoH25@*β*-CD was only 9.65 mm, significantly shorter than the other treatment groups (13.03 ~ 13.44 mm). This suggests that the supramolecule AoH25@*β*-CD possibly enhances the viscoelasticity of the droplets, making them less likely to slide off the surface, thereby improving leaf retention. Finally, the topological morphology on kiwifruit surface was inspected by SEM imaging. As

displayed in Fig. 2e, the AoH25 treatment group showed flaky aggregates that were suspended and unevenly distributed. In contrast, the AoH25@*β*-CD treatment group presented a uniform, well-dispersed arrangement of small particles, forming a dense coating on the kiwifruit surface without large lamellar precipitates. These findings indicate that AoH25@*β*-CD achieves superior wetting and deposition performance on the kiwifruit surface, laying the foundation for improved bioavailability.

AoH25@*β*-CD shows superior antifungal activity against kiwifruit soft rot

Kiwifruit soft rot, caused by pathogenic *B. dothidea*, poses a significant threat to kiwifruit production and storage. To assess the efficacy of versatile supramolecular fungicide AoH25@*β*-CD in controlling this disease, we conducted an activity assessment on infected kiwifruits. At a concentration of 100 μg mL^{-1}, kiwifruits treated with different fungicides were evaluated for their curative and protective effects. The control group, which received no treatment, exhibited prominent yellow lesions, indicative of severe infection. In contrast, kiwifruits treated with AoH25@*β*-CD showed markedly reduced lesion sizes and color intensity, suggesting a significant reduction in disease severity (Fig. 3a). Quantitative analysis of the control efficiency (Fig. 3b and c) revealed that AoH25@*β*-CD outperformed the commercial fungicides FP and AZX. Specifically, AoH25@*β*-CD demonstrated curative and protective efficacies of 85.3% and 88.5%, respectively. Those data notably exceeded those of FP (50.0% and 52.4%), AZX (61.8% and 65.4%), and single AoH25 (70.6% and 74.0%). The significantly enhanced efficacy of AoH25@*β*-CD probably attributes to the improved biocompatibility, droplet retention, and penetrability, thus achieving superior bioavailability. The current supramolecular system is green, efficient, and without using any traditional pesticide additives, minimizing unnecessary harm to our fragile ecosystems, food safety, and human health.

AoH25@*β*-CD enhances SDH inhibition and cell permeability

To verify whether the designed structures are potential SDH inhibitors, molecular docking and SDH inhibition activity as well as the microscopic morphology of fungal mycelium were tested. As shown in Fig. 4a and

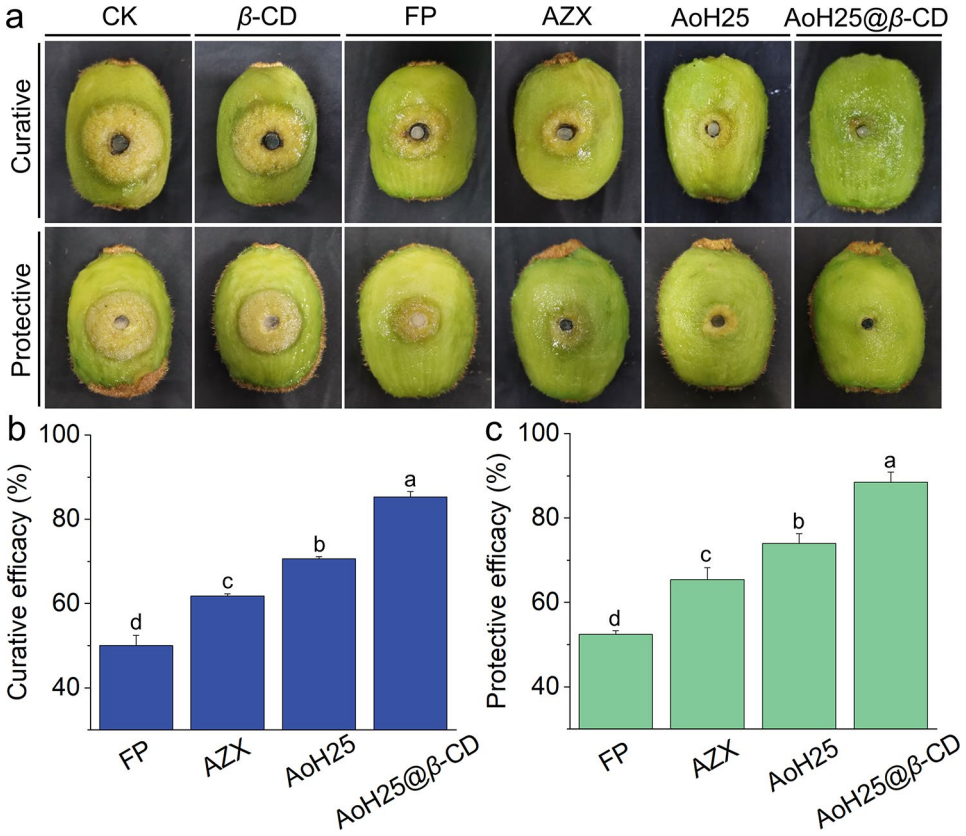

Fig. 3 (**a**) Photographic documentation and assessment of in vivo efficacy of AoH25@*β*-CD, AoH25 (0.1% Tween 20 additive), and commercial fungicides FP (0.1% Tween 20 additive) and AZX (0.1% Tween 20 additive) against kiwifruit soft rot at 100 μg mL^{-1}. (**b**) Curative and (**c**) protective efficacies expressed by histograms ($n = 3$, ANOVA; Tukey HSD; $p < 0.05$). Error bars indicate the means ± SD, different letters at each data indicate significant differences according to Duncan's multiple range test at $P < 0.05$

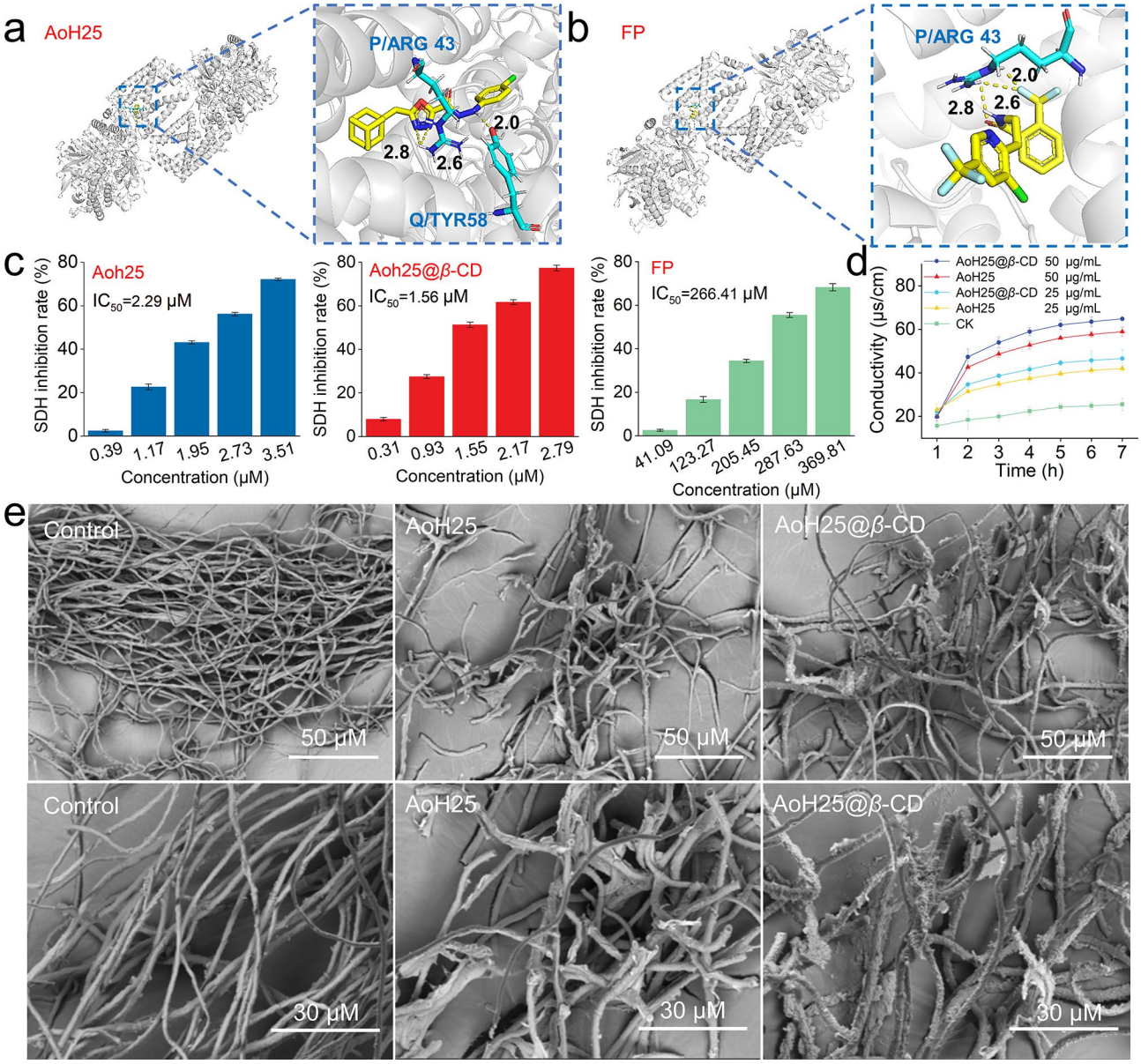

Fig. 4 Molecular docking and binding sites of compound AoH25 (**a**) and FP (**b**) with SDH (PDB entry: 2fbw). (**c**) The SDH inhibitory activity triggered by compound AoH25 and complex AoH25@*β*-CD, and FP. (**d**) The influence on the relative permeability of *B. dothidea* cell membrane triggered by AoH25, AoH25@*β*-CD, and FP at the doses of 50 and 25 μg mL^{-1} within 7 h. (**e**) The morphology of *B. dothidea* hyphae treated with different agents: blank control DMSO (0.1%), AoH25, and AoH25@*β*-CD at an effective concentration of 50 μg mL^{-1}

b, binding models of compounds AoH25 and FP with SDH (PDB code: 2FBW) were performed to investigate the possible binding interaction. The results show that AoH25 and FP enter the same binding pocket of SDH, but exhibit different binding sites. Interestingly, the 1,3,4-oxadiazole and hydrazide groups of AoH25 were able to form three hydrogen bonds with amino acid residues P/ARG43 (distances of 2.8 Å and 2.6 Å, from succinate dehydrogenase cytochrome b560 subunit) and Q/TRP58 (distance of 2.0 Å, from cytochrome succinate dehydrogenase [ubiquinone] cytochrome b small subunit), which was different from that of FP via fluorine atom and carbonyl group forming hydrogen bonds with amino acid residues of P/ARG43. Subsequently, the inhibition of SDH enzyme by different treatments at the same conditions was evaluated via SDH kit operating instructions (BC0955, Beijing Solarbio Science & Technology Co., Ltd.), and the corresponding IC_{50} was calculated separately (Fig. 4c). Intriguingly, the IC_{50} of AoH25, being 2.29 μM, was much lower than the positive control treatment FP (IC_{50}=266.41 μM). Significantly, the IC_{50} of AoH25@*β*-CD against SDH was even lower

at 1.56 μM. These evidences preliminarily indicate that the designed small molecule AoH25 as well as optimized supramolecular fungicide AoH25@β-CD are potential novel SDH inhibitors. Whereafter, the effects of AoH25 and AoH25@β-CD on the permeability of *B. dothidea* cell membrane were tested at different doses of 50 and 25 μg mL^{-1} (Fig. 4d). With the extension of treatment time, the relative seepage ratio of the cell membrane treated with AoH25@β-CD was higher than that of AoH25. For example, at a dose of 50 μg mL^{-1}, upon treating the fungal cell membrane for 5 h, the permeation rates of AoH25 and AoH25@β-CD treated groups were 56.1% and 62.1%, respectively, revealing that the AoH25@β-CD treated cells were more favorable for fungicide penetration and led to a relatively higher seepage ratio. Therefore, we inferred that the degree of damage to the cell membrane of *B. dothidea* by AoH25@β-CD exceeded that of AoH25. To test this conjecture, SEM was used to observe the *B. dothidea* hyphae treated with the same dose of AoH25 and AoH25@β-CD. As illustrated in Fig. 4e, for the black control, the *B. dothidea* hyphae were intact and smooth. The treatment of *B. dothidea* hyphae with AoH25 showed apparent shrinkage, entanglement, and folding, while the surface of *B. dothidea* hyphae treated with AoH25@β-CD exhibited significant distortion, deformity, and more flocculent aggregation. These investigations prove that the biocompatible supramolecular material AoH25@β-CD has an enhancive destruction effect on *B. dothidea* hyphae, thereby subduing their growth and reproduction. In conclusion, AoH25@β-CD is a potential SDH inhibitor with an admirable water-dispersibility, biocompatibility and bioavailability.

Excellent wettability of AoH25@β-CD on oilseed rape surface

The pathogenic *S. sclerotiorum* can cause the intractable oilseed rape sclerotinia, seriously harming the rapeseed industry [58, 59]. To extend the broad-spectrum applications of AoH25@β-CD for controlling other fungal infections, the droplet/foliage interface interaction, including the wetting, bouncing, sliding, and deposition properties on hydrophobic rape leaves, was investigated firstly. As shown in Fig. 5a, the related contact angles of water, β-CD and AoH25 were 122°, 116°, and 116.5°, respectively. In contrast, the contact angle of AoH25@β-CD afforded a smaller value of 104°, indicating that the self-assembled nanovesicles were more easily spread on the oilseed rape leaf surface. On the other hand, to visualize the distribution status of droplets on the leaf surface of oilseed rape, spraying experiments were conducted. Distinctly, spraying of AoH25@β-CD showed smaller sizes and greater densities on the leaves, showing the superior potential in practical applications. Later, the LHC of AoH25@β-CD was quantified, which is crucial for how much active ingredient can be deposited on the leaves (Fig. 5b). As a result, the LHC of AoH25@β-CD was 1.6-fold higher than that of AoH25, implying that the optimized supramolecular complex has better liquid retention performance. Similarly, the impact and sliding of fungicide droplets on the hydrophobic foliage can likewise lead to the loss of active ingredients and pollute the environment. To inspect this case, four kinds of droplets (water, β-CD, AoH25, AoH25@β-CD) were released at the same height of 15 cm. When these droplets impacted the surface of the rape leaf, the droplet diameter first spread to the maximum, retraction occurred randomly, and then accompanied by the conversion of kinetic energy into potential energy to detach from the leaf surface. Finally, the energy of droplet was exhausted to stay on the leaf surface of oilseed rape (Fig. 5c and Video S2). Encouragingly, AoH25@β-CD alleviates this encounter. To analyze the impact process more intuitively, the normalized rebound height (H_t/D_0) of droplets in this process were obtained (Fig. 5e), where H_t denotes the height of the droplet at different times, respectively, and D_0 denotes the initial diameter of the droplet. Across the droplets after the first occurrence of bouncing, AoH25@β-CD consistently had a lower bouncing height than water, β-CD and AoH25 throughout the process. For instance, at 15 ms, the H_t/D_0 value of AoH25@β-CD was 2.43, significantly lower than that of AoH25 (3.20), β-CD (3.44), and water (3.65), indicating that our designed supramolecular system effectively mitigates droplet bouncing behavior. Additionally, we inclined the oilseed rape leaves to observe the sliding behavior of droplets (Fig. 5d, Videos S3-S4). At an inclination angle of 30°, the normalized sliding distance (L_t/D_0) of AoH25@β-CD droplets at rest was 8.07, notably lower than those of AoH25 (8.67), β-CD (9.47), and water (9.89) (Fig. 5f). When the inclination angle was increased to 60°, the advantages of the supramolecular assembly became even more pronounced (Fig. 5g). After all droplets came to rest (52 ms), AoH25@β-CD exhibited a lower L_t/D_0 of 15.13, far lower than the other three components (22.98 ~ 23.22). This indicates that the constructed supramolecule demonstrates superior retention on inclined leaf surfaces, preventing easy sliding off. Finally, SEM imaging further illustrates the excellent deposition effect of AoH25@β-CD on oilseed rape leaves (Fig. 5h). In the control group, the leaf surface appears some intrinsic waxy layer structure. After treating with AoH25, piece-like structures were observed with a suspending, disheveled, and undeposited status. Magnetically, leaves treated with AoH25@β-CD demonstrate a significantly different deposition pattern. The surface is densely covered with uniformly distributed spherical particles, creating a continuous and cohesive layer. This finding again indicates a more effective and stable interface interaction between

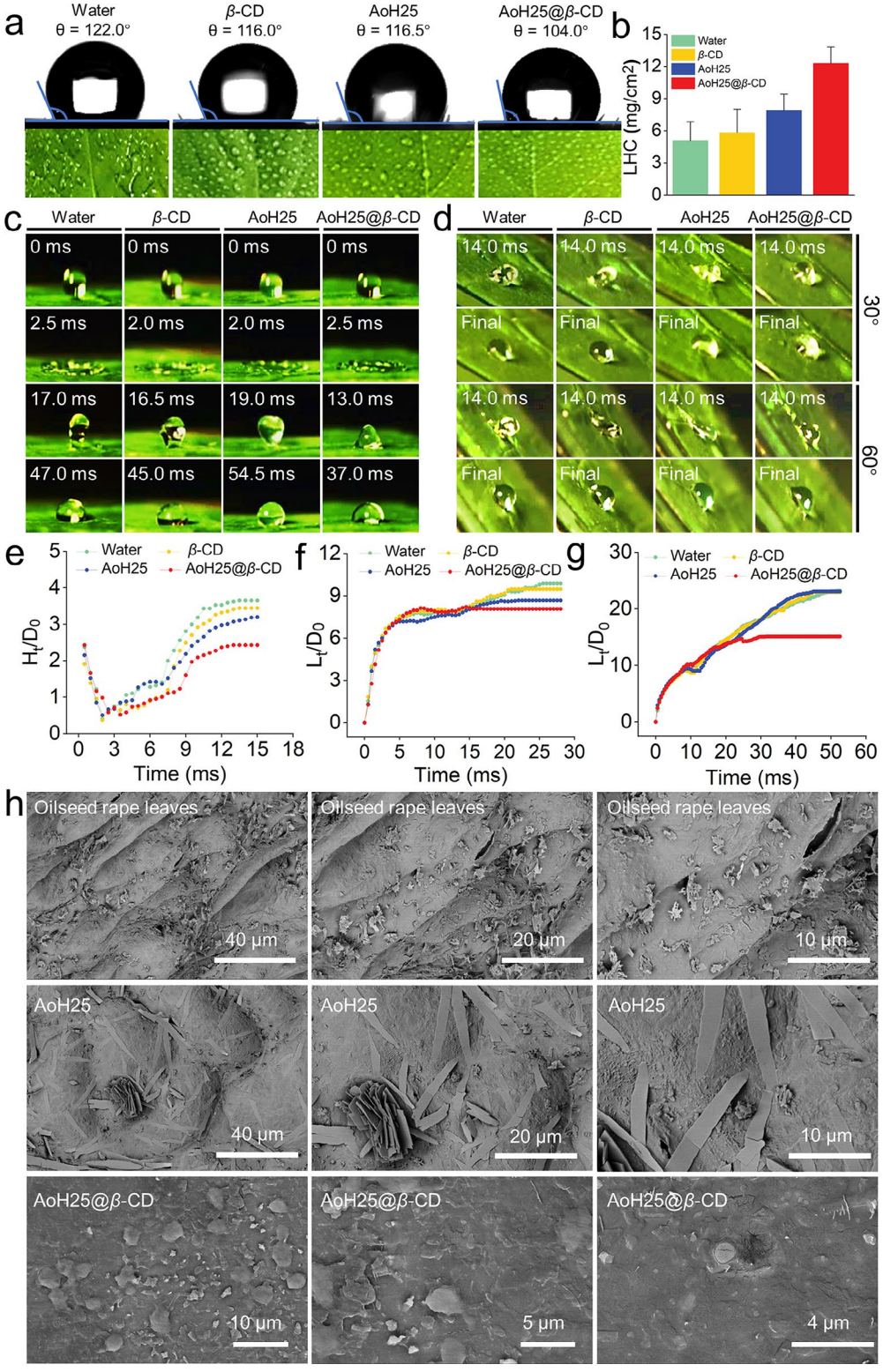

Fig. 5 (**a**) Contact angles of water, *β*-CD, AoH25, and AoH25@*β*-CD droplets on oilseed rape leaf at 200 μg mL^{-1}. (**b**) The liquid holding capacities (LHC) of AoH25@*β*-CD, AoH25 and *β*-CD after dipping in oilseed rape leaf at 200 μg mL^{-1}. (**c**-**d**) The oilseed rape leaf is placed at 0°, 30° and 60°, the related droplets are released at a height of 15 cm and recorded by a high-speed camera, scale: 2.0 mm. (**e**) Normalized height of water, *β*-CD, AoH25, and AoH25@*β*-CD droplets (H_t/D_0) over time. (**f**) and (**g**) Normalized sliding distance of water, *β*-CD, AoH25, and AoH25@*β*-CD droplets (L_t/D_0) over time. (**h**) SEM images of control (oilseed rape leaf), AoH25 and AoH25@*β*-CD deposited on oilseed rape leaf surface at 200 μg mL^{-1}

AoH25@*β*-CD and the leaf surface, thereby enhancing the fungicide retention and ultimate utilization ratio. Based on the above-mentioned evidences, it is workable to utilize an intelligent host-guest supramolecular strategy to optimize the physicochemical and topological structures of active ingredients, eventually realizing the enhancement of biocompatibility and liquid/solid interface interactions.

AoH25@*β*-CD shows enhanced in vivo antifungal activity against rape sclerotinia rot

Given the excellent wetting, retention, and biocompatibility of AoH25@*β*-CD, we evaluated its effectiveness against *S. sclerotiorum*-induced sclerotinia rot in oilseed rape. At a lower concentration of 100 μg mL^{-1}, AoH25@*β*-CD treated groups showed significantly reduced lesions, demonstrating superior curative and protective efficacies of 87.2% and 84.6%, respectively (Fig. 6a-c). This effect was quite superior to those of commercial fungicides FP + 0.1% Tween-20 (48.7% and 40.2%) and AZX + 0.1% Tween-20 (76.7% and 68.8%) as well as the single guest molecule AoH25 + 0.1% Tween-20 (77.8% and 72.7%). These outcomes indicate that AoH25@*β*-CD exhibits remarkably enhanced control efficiency against *sclerotinia* rot. To preliminarily assess the environmental impact of AoH25@*β*-CD in terms of off-target effects, the acute toxicity test toward the representative earthworms was performed. As shown in Fig. S2, all the earthworms were alive with a survival rate of 100% at 12 μg mL^{-1} after treating with AoH25@*β*-CD, verifying the biosafety of AoH25@*β*-CD to current non-target organisms.

Conclusion

Updating the structure of existing SDHIs and synchronously realizing the efficient utilization are challenging in creating new fungicide. This study developed a novel supramolecular SDH inhibitor—AoH25@*β*-CD by utilizing the flexible host-guest supramolecular strategy, demonstrating remarkable antifungal efficacy and superior foliar deposition properties. Through this manipulation, the water-solubility and bioavailability of the active molecule AoH25 are markedly improved. Comprehensive evaluation found that AoH25@*β*-CD could prominently improve the droplet/foliage interface interaction, such as reducing contact angles and enhancing wettability and retention, laying the foundation for enhancing fungicide utilization. Molecular docking and SDH inhibition assays reveal that AoH25@*β*-CD was a potentially potent

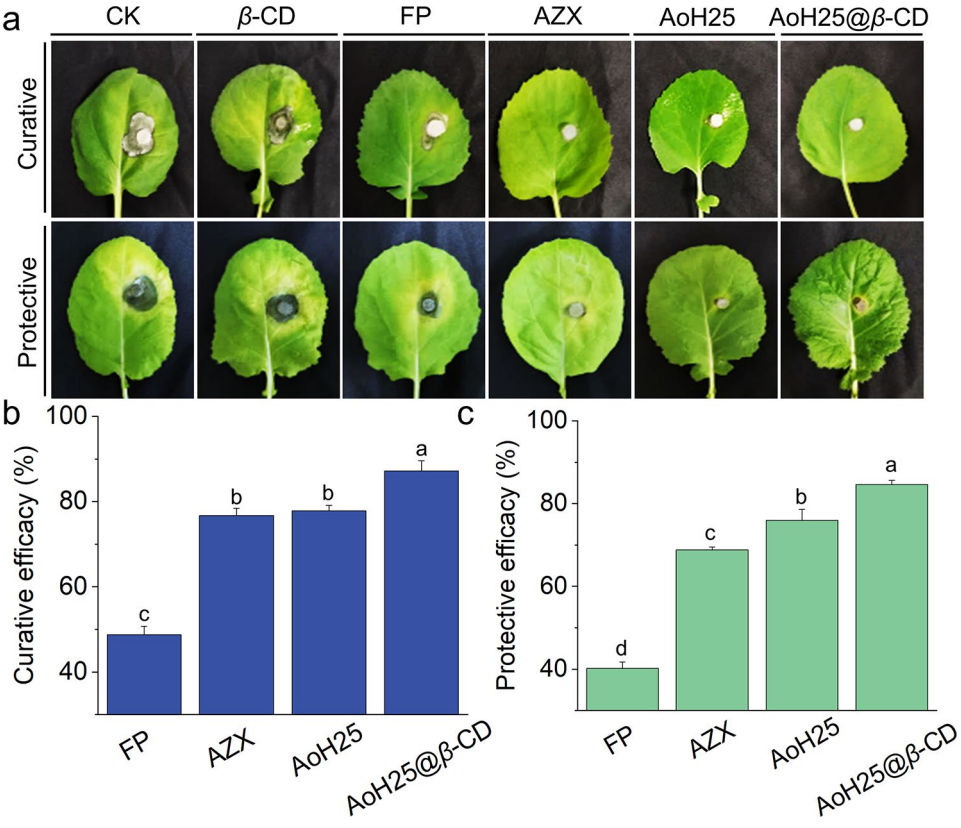

Fig. 6 (**a**) Photographic documentation and assessment of in vivo efficacy of AoH25, AoH25@*β*-CD, and commercial fungicides FP and AZX against sclerotinia stem rot at 100 μg mL^{-1}. (**b**) Curative and (**c**) protective efficacies expressed by histograms ($n = 3$, ANOVA; Tukey HSD; $p < 0.05$). Error bars indicate the means ± SD, different letters at each data indicate significant differences according to Duncan's multiple range test at $P < 0.05$

SDH inhibitor with an IC_{50} value of 1.56 μM, superior to those of FP (244.41 μM) and AoH25 (2.29 μM). Additionally, AoH25@β-CD increases the permeability of cell membranes in *B. dothidea*, promoting the better penetration of active ingredients into fungal strains. Further studies demonstrated that AoH25@β-CD provided superior curative and protective effects against kiwifruit soft rot and sclerotinia rot in oilseed rape. This operable supramolecular optimization strategy addresses critical challenges related to fungicide innovation and efficient utilization. These advancements set a promising foundation for the development of next-generation plant disease management solutions, emphasizing both efficacy and sustainability.

Supplementary Information

The online version contains supplementary material available at https://doi.org/10.1186/s12951-024-02849-y.

Supplementary Material 1

Acknowledgements
We acknowledge funds from the National Key Research and Development Program (2022YFD1700300), Innovation Program for High-level Talents of Guizhou Province (No. GCC[2023]008), Guizhou Provincial S&T Project (ZK[2022]017), Research and Innovation Team of Guizhou University (Guidakechuangtuan[2023]03), Natural Science Special Project of Guizhou University (Guidazhuanjihe[2024]02), Central Government Guides Local Science and Technology Development Fund Projects (Qiankehezhongyindi (2023) 001), and the Program of Introducing Talents of Discipline to Universities of China (111 Program, D20023).

Author contributions
Study design: Dengxuan Guo and Peiyi Wang. Supervision: Peiyi Wang. Performed experiments: Dengxuan Guo and Li Song. Data analysis: Dengxuan Guo, Jinghan Yang, and Peiyi Wang. Visualization: Xinyu He, Pan Liu, and Jinghan Yang. Writing-original draft: Jinghan Yang. Writing—review and editing: Peiyi Wang.

Data availability
No datasets were generated or analysed during the current study.

Declarations

Competing interests
The authors declare no competing interests.

Author details
[1]State Key Laboratory of Green Pesticide, Key Laboratory of Green Pesticide and Agricultural Bioengineering, Ministry of Education, Center for Research and Development of Fine Chemicals of Guizhou University, Guiyang 550025, China

Received: 26 July 2024 / Accepted: 7 September 2024
Published online: 20 September 2024

References

1. Strange RN, Scott PR. Plant Disease: a threat to global Food Security. Annu Rev Phytopathol. 2005;43:83–116.
2. Fisher MC, Hawkins NJ, Sanglard D, Gurr SJ. Worldwide emergence of resistance to antifungal drugs challenges human health and food security. Science. 2018;360:739–42.
3. Coussens NP, Molinaro AL, Culbertson KJ, Peryea T, Zahoránszky-Köhalmi G, Hall MD, Daines DA. Better living through chemistry: addressing emerging antibiotic resistance. Exp Biol Med. 2018;243:538–53.
4. Brauer VS, Rezende CP, Pessoni AM, De Paula RG, Rangappa KS, Nayaka SC, Gupta VK, Almeida F. Antifungal agents in Agriculture: friends and Foes of Public Health. Biomolecules. 2019;9:521.
5. Tudi M, Daniel Ruan H, Wang L, Lyu J, Sadler R, Connell D, Chu C, Phung DT. Agriculture Development, Pesticide Application and its impact on the Environment. Int J Environ Res Public Health. 2021;18:1122.
6. Bai Y, Wang L, Yuan X. Pesticide control, physical control, or biological control? How to manage forest pests and diseases more effectively. Front Ecol Evolut. 2023;11:1200268.
7. Li S, Li X, Zhang H, Wang Z, Xu H. The research progress in and perspective of potential fungicides: succinate dehydrogenase inhibitors. Bioorg Med Chem. 2021;50:116476.
8. Dalla Pozza E, Dando I, Pacchiana R, Liboi E, Scupoli MT, Donadelli M, Palmieri M. Regulation of succinate dehydrogenase and role of succinate in cancer. Semin Cell Dev Biol. 2020;98:4–14.
9. Cao K, Xu J, Cao W, Wang X, Lv W, Zeng M, Zou X, Liu J, Feng Z. Assembly of mitochondrial succinate dehydrogenase in human health and disease. Free Radical Bio Med. 2023;207:247–59.
10. Hospital CD, Tête A, Debizet K, Imler J, Tomkiewicz-Raulet C, Blanc EB, Barouki R, Coumoul X, Bortoli S. SDHi fungicides: an example of mitotoxic pesticides targeting the succinate dehydrogenase complex. Environ Int. 2023;180:108219.
11. Li Z, Zhang X, Wang Y, Zheng Z, Zhang C, Wu T, Wu Y, Gao Y, Du F. Improved method to Characterize Leaf surfaces, Guide Adjuvant Selection, and improve glyphosate efficacy. J Agric Food Chem. 2023;71:1348–59.
12. Rehfus A, Miessner S, Achenbach J, Strobel D, Bryson R, Stammler G. Emergence of succinate dehydrogenase inhibitor resistance of *Pyrenophora teres* in Europe. Pest Manag Sci. 2016;72:1977–88.
13. Shao W, Sun J, Zhang X, Chen C. Amino acid polymorphism in Succinate Dehydrogenase Subunit C involved in Biological Fitness of *Botrytis Cinerea*. Mol Plant Microbe Interact. 2020;33:580–9.
14. Zhu J, Li J, Ma D, Gao Y, Cheng J, Mu W, Li B, Liu F. SDH mutations confer complex cross-resistance patterns to SDHIs in *Corynespora Cassiicola*. Pesticide Biochem Physiol. 2022;186:105157.
15. Landschoot S, Carrette J, Vandecasteele M, De Baets B, Höfte M, Audenaert K, Haesaert G. Boscalid-resistance in *Alternaria alternata* and *Alternaria solani* populations: an emerging problem in Europe. Crop Prot. 2017;92:49–59.
16. Shima Y, Ito Y, Kaneko S, Hatabayashi H, Watanabe Y, Adachi Y, Yabe K. Identification of three mutant loci conferring carboxin-resistance and development of a novel transformation system in *aspergillus oryzae*. Fungal Genet Biol. 2009;46:67–76.
17. Pei Q, Hu X, Wang L, Liu S, Jing X, Xie Z. Cyclodextrin/Paclitaxel dimer assembling vesicles: reversible morphology transition and Cargo Delivery. ACS Appl Mater Interfaces. 2017;9:26740–8.
18. Zheng K, Liu X, Liu H, Dong D, Li L, Jiang L, Huang M, Ding C. Novel pH-Triggered doxorubicin-releasing nanoparticles self-assembled by Functionalized β-Cyclodextrin and Amphiphilic Phthalocyanine for Anticancer Therapy. ACS Appl Mater Interfaces. 2021;13:10674–88.
19. Bian Q, Wang W, Wang S, Wang G. Light-triggered specific Cancer cell release from Cyclodextrin/Azobenzene and aptamer-modified substrate. ACS Appl Mater Interfaces. 2016;8:27360–7.
20. Tang G, Tian Y, Gao Y, Zhou Z, Chen X, Li Y, Yu X, Wang H, Li X, Cao Y. Supramolecular Self-Assembly of herbicides with reduced risks to the Environment. ACS Nano. 2022;16:4892–904.
21. Su C, Liu S, Cao S, Yin S, Zhou C, Gao S, Jia C, Ji Y, Liu Y. Self-assembled bovine serum albumin nanoparticles as pesticide delivery vectors for controlling trunk-boring pests. J Nanobiotechnol. 2020;18:1–14.
22. Nadiminti PP, Liu Q, Vanjari LK, Dong YD, Boyd BJ, Cahill DM. Novel self-assembling conjugates as vectors for agrochemical delivery. J Nanobiotechnol. 2018;16:1–15.
23. Ma R, Zheng YD, Tian HW, Chen MM, Yue YX, Bian Q, Li HB, Guo DS. A general supramolecular adjuvant for pesticides based on host–guest recognition. Pest Manag Sci. 2023;79:3133–40.
24. Xie H, Yu G, Wang X, Chu D, Song C, Wang P, Dai K, Li J, Yin H. Sea urchin-like nanocarrier for enhancing pesticide retention and rain fastness on hydrophobic and hydrophilic crop foliage. Chem Eng J. 2024;490:151901.
25. Hădărugă NG, Bandur GN, David I, Hădărugă DI. A review on thermal analyses of cyclodextrins and cyclodextrin complexes. Environ Chem Lett. 2018;17:349–73.

26. Wang HJ, Xing WW, Yu ZH, Li YX, Zhang HY, Yu Q, Zhu H, Wang YY, Liu Y. Cucurbit[7]uril confined phenothiazine bridged bis (bromophenyl pyridine) activated NIR luminescence for lysosome imaging. Chin Chem Lett. 2024;35:109183.
27. Adeli F, Abbasi F, Babazadeh M, Davaran S. Thermo/pH dual-responsive micelles based on the host–guest interaction between benzimidazole-terminated graft copolymer and β-cyclodextrin-functionalized star block copolymer for smart drug delivery. J Nanobiotechnol. 2022;20:91.
28. Song Q, Mei L, Zhang X, Xu P, Dhinakaran MK, Li H, Yang G. Spreading of benquitrione droplets on superhydrophobic leaves through pillar[5]arene-based host–guest chemistry. Chem Commun. 2020;56:7593–6.
29. Decool G, Kfoury M, Paitel L, Sardo A, Fourmentin S. Cyclodextrins as molecular carriers for biopesticides: a review. Environ Chem Lett. 2023;22:321–53.
30. Pandey A. Cyclodextrin-based nanoparticles for pharmaceutical applications: a review. Environ Chem Lett. 2021;19:4297–310.
31. Loh GOK, Tan YTF, Peh K-K. Enhancement of norfloxacin solubility via inclusion complexation with β-cyclodextrin and its derivative hydroxypropyl-β-cyclodextrin. Asian J Pharm Sci. 2016;11:536–46.
32. Crini G, Fourmentin S, Fenyvesi É, Torri G, Fourmentin M, Morin-Crini N. Cyclodextrins, from molecules to applications. Environ Chem Lett. 2018;16:1361–75.
33. Li W, Xu W, Zhang S, Li J, Zhou J, Tian D, Cheng J, Li H. Supramolecular Biopharmaceutical Carriers based on host–guest interactions. J Agric Food Chem. 2022;70:12746–59.
34. Wang JW, Yu KX, Ji XY, Bai H, Zhang WH, Hu X, Tang G. Structural insights into the host–guest complexation between β-Cyclodextrin and Bio-conjugatable adamantane derivatives. Molecules. 2021;26:2412.
35. Ji QT, Mu XF, Hu DK, Fan LJ, Xiang SZ, Ye HJ, Gao XH, Wang PY. Fabrication of host–guest complexes between adamantane-functionalized 1,3,4-Oxadiazoles and β-Cyclodextrin with Improved Control Efficiency against Intractable Plant Bacterial diseases. ACS Appl Mater Interfaces. 2022;14:2564–77.
36. Jiang J, Zhu Z, Niu X, Yan Y, Li Y, Song D, Tang S, Xing J. Construction and synthesis of tricyclic matrinic derivatives against influenza a virus by privileged structure strategy. Pharmazie. 2019;74:265–9.
37. Al-Wahaibi LH, Alvarez N, Blacque O, Veiga N, Al-Mutairi AA, El-Emam AA. Synthesis and structure insights of two novel broad-spectrum antibacterial candidates based on (E)-*N*′-[(Heteroaryl)methylene]adamantane-1-carbohydrazides. Molecules. 2020;25:1–17.
38. Cheng AV, Kim W, Escobar IE, Mylonakis E, Wuest WM. Structure–activity relationship and Anticancer Profile of Second-Generation Anti-MRSA Synthetic retinoids. ACS Med Chem Lett. 2019;11:393–7.
39. Dong J, Chen W, Qin D, Chen Y, Li J, Wang C, Yu Y, Feng J, Du X. Cyclodextrin polymer-valved MoS2-embedded mesoporous silica nanopesticides toward hierarchical targets via multidimensional stimuli of biological and natural environments. J Hazard Mater. 2021;419:126404.
40. An J, Pan N, Liu C, Chen H, Fei Q, Gan X, Wu W. Synthesis, biological evaluation, and molecular docking of novel ferulic acid derivatives containing a 1,3,4-oxadiazole thioether and trifluoromethyl pyrimidine skeleton. RSC Adv. 2024;14:16218.
41. Fei Q, Liu C, Luo Y, Chen H, Ma F, Xu S, Wu W. Rational design, synthesis, and antimicrobial evaluation of novel 1,2,4-trizaole-substituted 1,3,4-oxadiazole derivatives with a dual thioether moiety. Mol Divers. 2024. https://doi.org/10.1007/s11030-024-10848-2.
42. Pan N, Liu C, Wu R, Fei Q, Wu W. Novel pyrimidine derivatives bearing a 1,3,4-Thiadiazole skeleton: design, synthesis, and antifungal activity. Front Chem. 2022;10:1–5.
43. Gelmboldt V, Ognichenko L, Shyshkin I, Kuz'min V. QSPR models for water solubility of ammonium hexafluorosilicates: analysis of the effects of hydrogen bonds. Struct Chem. 2020;32:309.
44. Geetha-Loganathan P, Gibbons J. Processing embryo, Eggshell, and Fungal Culture for scanning Electron Microscopy. Jove-J Vis Exp. 2019. https://doi.org/10.3791/60018.
45. Yin YM, Sun ZY, Wang DW, Xi Z. Discovery of Benzothiazolylpyrazole-4-Carboxamides as potent succinate dehydrogenase inhibitors through active Fragment Exchange and Link Approach. J Agric Food Chem. 2023;71:14471.
46. Hammoudi Halat D, Younes S, Mourad N, Rahal M. Allylamines, Benzylamines, and fungal cell permeability: a review of mechanistic effects and usefulness against fungal pathogens. Membranes. 2022;12:1–19.
47. Feng J, Chen W, Liu Q, Chen Z, Yang J, Yang W. Development of abamectin-loaded nanoemulsion and its insecticidal activity and cytotoxicity. Pest Manag Sci. 2020;76:4192.
48. Dai H, Yang J, Fan L, Luo M, Wang P. Excellent Foliar deposition of cyclodextrin-encapsulated Furyl/Thienyl-Engineered ingredients: Novel Effective Supramolecular agrochemicals for combating plant bacterial and fungal infections. Adv Funct Mater. 2024. https://doi.org/10.1002/adfm.202403823.
49. Wu Y, Bao Z, Zhang S, Liu R, Ping Y, Ma M, Gao Y, He C, Wu T, Ma Y, Zhang C, Du F. Salinity-driven interface self-assembly of a biological amphiphilic emulsifier to form stable Janus core–Shell Emulsion for Enhancing Agrichemical Delivery. ACS Nano. 2024;18:9486.
50. Pan H, Zhong C, Xia L, Li W, Wang Z, Deng L, Li L. Long C-a, antifungal activity of natamycin against kiwifruit soft rot caused by *Botryosphaeria Dothidea* and potential mechanisms. Sci Hort. 2022;305:111344.
51. Liang W, Xie Z, Cheng J, Xiao D, Xiong Q, Wang Q, Zhao J, Gui W. A light-triggered pH-Responsive Metal-Organic Framework for Smart Delivery of Fungicide to Control *Sclerotinia* Diseases of Oilseed Rape. ACS Nano. 2021;15:6987.
52. Long Z, Yang L, Zhang J, Liu S, Jiao X, Wang P, Zhu J, Shao W, Liu L, Yang S. Fabrication of versatile pyrazole hydrazide derivatives bearing a 1,3,4-Oxadiazole core as Multipurpose Agricultural Chemicals against Plant Fungal, Oomycete, and bacterial diseases. J Agric Food Chem. 2021;69:8380.
53. Li M, Wang W, Cheng X, Wang Y, Chen Y, Gong J, Chang X, Lv X. Design, synthesis, and evaluation of Antifungal Bioactivity of Novel Pyrazole Carboxamide thiazole derivatives as SDH inhibitors. J Agric Food Chem. 2023;71:11365–72.
54. Wang Q, Chen Y, Liu Y. Supramolecular ternary polymer mediated by cucurbituril and cyclodextrin. Polym Chem. 2013;4:4192.
55. Car Ž, Kodrin I, Požar J, Ribić R, Kovačević D, Peroković VP. Experimental and computational study of the complexation of adamantyl glycosides with β-cyclodextrin. Tetrahedron. 2013;69:8051–63.
56. Deng C, Cao C, Zhang Y, Hu J, Gong Y, Zheng M, Zhou Y. Formation and stabilization mechanism of β-cyclodextrin inclusion complex with C10 aroma molecules. Food Hydrocoll. 2022;123:107013.
57. Zhang Z, Chen T, Yin X, Wang W, Li W, Chen X, Ma J, Long Y. Honokiol inhibits *Botryosphaeria Dothidea*, the causal pathogen of kiwifruit soft rot, by targeting membrane lipid biosynthesis. Pest Manag Sci. 2023;80:1779–94.
58. Jian H, Ma J, Wei L, Liu P, Zhang A, Yang B, Li J, Xu X, Liu L. Integrated mRNA, sRNA, and degradome sequencing reveal oilseed rape complex responses to *Sclerotinia Sclerotiorum* (Lib.) Infection. Sci Rep. 2018;8:10987.
59. Ding LN, Li T, Guo XJ, Li M, Liu XY, Cao J, Tan XL. *Sclerotinia* Stem Rot Resistance in Rapeseed: recent progress and future prospects. J Agric Food Chem. 2021;69:2965–78.

Publisher's note